AIAA JOURNAL
Vol. 37, No. 7, July 1999

Effects of Perpendicular Blade–Vortex Interaction, Part 1: Turbulence Structure and Development

K. S. Wittmer* and W. J. Devenport†
Virginia Polytechnic Institute and State University, Blacksburg, Virginia 24061-0203

Three-component velocity and turbulence measurements were performed to document the turbulent flowfield produced downstream of an airfoil encountering an intense streamwise vortex. This configuration serves as a model for perpendicular blade–vortex interactions, which commonly occur in helicopter rotor flows. In the first part of a two-part paper, detailed measurements and analysis of a single flow—that produced by a vortex passing $\frac{1}{8}$th chord from the blade—are presented with the objective of revealing the physics and providing a computational test case. It is shown that the vortex passes the blade without immediate change in the form and structure of its core. However, outside the core the flow is modified by the blade wake, which contains negative streamwise vorticity shed as a result of the angle-of-attack distribution induced on the blade by the vortex. This negative vorticity and the turbulent motions of the blade wake then appear to trigger the turbulent decay of the vortex core, resulting in an increase in its size, reduction in its strength, and loss of circulation as its vorticity is partially canceled. As the core decays, the circulating velocity field outside it winds up the remainder of the blade wake, further increasing the size of the turbulent region in which the core has become embedded. A simple theoretical model predicts the circulation distribution on the blade in the presence of the vortex and, thus, the strength of the negative vorticity shed into the blade wake.

Nomenclature

b	= blade span between tunnel walls, 1.85 m
c	= chord length, 0.203 m
f	= frequency, Hz
G_{uu}	= u velocity autospectra
h	= distance from the coordinate system origin to the tunnel wall; see Fig. 8
k	= turbulence kinetic energy, $\frac{1}{2}(\overline{u^2} + \overline{v^2} + \overline{w^2})$
L_w	= length scale of generator wake
P	= turbulence kinetic energy production
r	= radial distance from vortex core center
r_1	= vortex core radius measured from the core center to the point of peak tangential velocity
U	= mean velocity in the x direction
U_d	= axial velocity deficit at vortex core center
U_w	= velocity scale of generator wake
U_∞	= freestream velocity
u, v, w	= fluctuating velocities in the x, y, z directions, respectively
V_{θ_1}	= peak tangential velocity of vortex
x, y, z	= coordinates defined in Fig. 1
α	= angle of attack, positive for right-hand rotation about negative y axis of Fig. 1
α_b	= geometric angle of attack of the blade
α_v	= angle of attack of the blade induced by the vortex
Γ	= circulation
Γ_b	= blade circulation
Γ_0	= root circulation of the vortex generator calculated using lifting line theory
Γ_1	= vortex core circulation defined as $2\pi r_1 V_{\theta_1}$
Δ	= blade–vortex separation in the z direction
$\Delta C_{L_{\max}}$	= maximum change in lift coefficient
Ω_x	= mean axial vorticity

Received 4 December 1997; revision received 16 January 1999; accepted for publication 23 January 1999.

*Research Associate, Department of Aerospace and Ocean Engineering; currently Handling Qualities Engineer, Sikorsky Aircraft Corporation, Stratford, CT 06615.

†Associate Professor, Department of Aerospace and Ocean Engineering. Senior Member AIAA.

Introduction

An important component of helicopter rotor flows is the interaction of the blades with their own vortex wakes. These interactions are usually thought of in terms of their acoustic effects, specifically the impulsive and broadband noise that they generate. However, they also have significant fluid dynamic effects on the development of the vortex and the flow surrounding it. When the same vortex suffers multiple interactions with the successive blades, these fluid dynamic effects can feed back significantly into both the acoustics and aerodynamics.

Impulsive noise is generated as a consequence of the unsteady lift experienced during parallel blade vortex interactions (BVIs). To predict this noise requires accurate knowledge of the vortex parameters, specifically the vortex core size, strength, and circulation distribution.[1–4] Broadband noise is defined by Brooks et al.[5] as the midfrequency noise due to blade interaction with turbulent portions of the blade wakes and is, thus, referred to as *blade wake interaction (BWI) noise*. To predict broadband noise requires information on the extent and intensity of the turbulent field encountered by the blade. It was originally believed that BWI noise was generated during perpendicular BVIs by the turbulence present in undisturbed blade wakes and tip vortices. However, after measuring the turbulence and spectral structure of an undisturbed vortex wake and incorporating the results into the BWI scheme of Glegg,[6] Glegg and Devenport[7] found the turbulence of the undisturbed wake to be simply insufficient to acount for the vast bulk of the noise produced. Wittmer et al.[8] and Devenport et al.[9] showed that this discrepancy can be accounted for by including the effects of a prior perpendicular BVI on the turbulence structure. Thus, it appears that multiple interactions are a key ingredient of BWI noise generation.

Although there have been a number of previous experimental studies on the effects of perpendicular interactions (see Ref. 10 for a review), these have tended to concentrate on effects on the blade aerodynamics or noise generation process itself. The work of Wittmer et al.,[8] is unique in presenting turbulence measurements downstream of the interaction. They examined the development of a vortex following a perpendicular interaction occuring near a blade tip. They found that the interaction results in a large, intense region of turbulence in the vicinity of the vortex and a region of negative vorticity shed by the blade in response to the spanwise variations in angle of attack produced by the passing vortex. The interaction also greatly increased the rates of vortex core growth and tangential velocity decay downstream of the blade.

Although the results of Wittmer et al.[8] are complicated by the presence of the interaction blade tip vortex and cover only a limited set of conditions, they conclusively show that a perpendicular blade vortex interaction can substantially alter the character and development of a trailing vortex even when the vortex core passes some distance from the blade. Thus, perpendicular BVIs can substantially influence the BWI or BVI noise generated by subsequent interactions.

The present study forms an extension of Ref. 8 with two objectives. First is to document the turbulence structure of the flow downstream of a perpendicular interaction in sufficient detail (and without the complication of an additional tip vortex) to unambiguously reveal the underlying physics of the flow and provide a suitable database for the development of computational fluid dynamics (CFD) prediction methods. Second is to document the influence of perpendicular interaction on the key parameters of the vortex (core size, strength, profile) used in BVI and BWI noise prediction methods, as functions of the most important variables defining the interaction, i.e., blade–vortex separation, blade angle of attack, and vortex strength. Such data are needed for the development of empirical methods to account for the influence of prior perpendicular BVIs in BVI and BWI noise prediction schemes.

This paper is presented in two parts. Part 1 addresses the first objective with the presentation of detailed measurements and analysis of a single flow: that generated by a vortex passing one-eighth of a chord from the pressure side of a two-dimensional blade. Part 2 (Ref. 11), addressing the second objective, presents measurements for a broad range of flows that cover substantial variations in all of the important variables defining the interaction.

Apparatus and Instrumentation

Wind Tunnel

Experiments were performed in the Virginia Polytechnic Institute and State University Stability Wind Tunnel, a closed-circuit facility powered by a 600-hp axial fan. The test section has a square cross section 1.83 × 1.83 m and a length of 7.33 m. Flow in the empty test section is nearly uniform with a turbulence intensity of less than 0.1% at 40 m/s, the freestream velocity used for this study. A slight favorable pressure gradient ($\partial C_p/\partial x = -0.003$/m) exists along the test section due to boundary-layer growth, which causes some convergence of the streamlines. Flow angles are small near the middle of the section but increase to about 2 deg near the walls.[12]

The freestream dynamic pressure and flow temperature are monitored continuously during operation of the wind tunnel. The former is measured using a pitot-static probe located at the upstream end of the test section connected to a Barocell electronic manometer. The latter is sensed using an Omega thermocouple located within the test section boundary layer; there is no significant temperature gradient across the boundary layer.

Blades

Untwisted NACA 0012 blades were used: one to generate the vortex and the other to interact with it. Both had a rectangular planform of 0.203-m chord. Effective boundary-layer trips were placed on both blades. These consisted of 0.5-mm-diam glass beads glued in a random pattern along the entire span between the 20% and 40% chord locations. The resulting turbulent boundary layers documented by Devenport et al.[7] are shown in Table 1. The vortex generator blade (hereafter referred to as the generator) was mounted vertically as a half-wing at the center of the upper wall of the test section entrance with 0.879 m protruding into the flow (Fig. 1). The

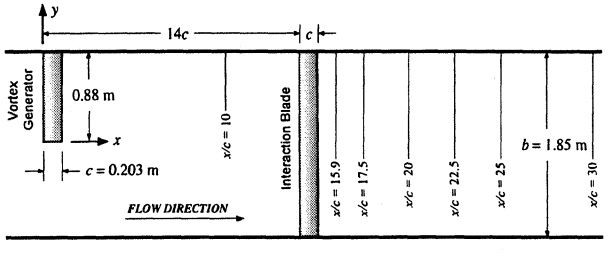

Fig. 1 Wind-tunnel schematic and coordinate system. Coordinate z is directed out of the paper.

Table 1 Boundary-layer properties for the generator at 5 deg estimated from near-wake profile measurements at $x/c = 1.05$, $y/c = 1.2$

Parameter	Pressure side	Suction side
$\delta/c \times 100$	4.35	6.22
$\delta^*/c \times 100$	0.99	1.61
$\theta/c \times 100$	0.58	0.87
Re_θ	2900	4355

interaction blade was also mounted vertically. It completely spanned the test section 14c downstream of the vortex generator. A full-span blade was used to eliminate the complicating effects of an additional blade tip vortex, which would have been shed otherwise. For Part 1, both blades were set at angles of attack of 5 deg. Helium bubble flow visualization was used to determine the separation between the generator tip vortex and the interaction blade. (By being lighter than air, helium filled soap bubbles centrifuge into the vortex core, marking it clearly.) The interaction blade was first positioned as close as possible to the situation where the generator tip vortex core stagnates on its leading edge. Then it was moved 0.125c in the negative z direction so that the generator vortex passed to the pressure side. We define this as a blade–vortex separation Δ of $-0.125c$.

Hot-Wire Anemometry

Miniature four-sensor hot-wire probes were used for velocity measurements. Four-sensor probes consisting of two orthogonal X-wire arrays, normally associated with vorticity measurements,[13] are capable of simultaneous three-component velocity measurements from a relatively compact measurement volume and appear to overcome some of the gradient error problems associated with triple wire probes.

The probes were manufactured by Auspex Corporation (type AVOP-4-100). Eight stainless-steel tapered prongs (75 μm in diameter at their tips) position the wires some 40 mm upstream of the main part of the probe. The sensors are etched tungsten wire of 5 μm diam with an approximate length of 0.8 mm giving a length to diameter ratio of 160. The measurement volume of the probes is approximately 0.5 mm^3. The sensors are arranged as two orthogonal X-wire arrays with each wire inclined at a nominal 45-deg angle to the probe axis.

Hot-wire sensors were operated separately using Dantec 56C17/56C01 constant temperature anemometer units. Anemometer bridges were optimized to give a frequency response greater than 25 kHz. The output voltages from the anemometer bridges were recorded by an IBM AT compatible computer using an Analogic 12-bit HSDAS-12 A/D converter, which contains four separate converters. Hot-wire signals were buffered by four buck-and-gain amplifiers with calibrated filters to limit their frequency response to 50 kHz there by providing high-frequency noise attenuation. Voltage outputs from a digital thermometer and pressure transducer were also sampled by the A/D converter.

Probes were calibrated frequently for velocity using King's law to correlate the wire output voltages with the cooling velocities. Velocity components were determined from the cooling velocities by means of a direct angle calibration. To generate this calibration, the probe was pitched and yawed over all likely flow angles in a TSI calibrator jet. Comparing the known pitch and yaw angles with the probe outputs gives the true relationship between the cooling velocities and the flow angle. A complete description of the hot-wire method used can be found in Ref. 14.

Uncertainty estimates based on 20:1 odds for velocity measurements made with this hot-wire measurement system are contained in Table 2.

Results and Discussion

Measurements are presented in the wind-tunnel aligned coordinate system (x, y, z), shown in Fig. 1, unless otherwise indicated. Coordinate x is measured downstream from the generator leading edge, y inboard from its tip, and z from the quarter chord line so as to complete the right-handed system. The mean velocity components U, V, and W and fluctuating components u, v, and w are defined

in the x, y, and z directions, respectively. In this system, the leading edge of the interaction blade is at $x/c = 14$. All measurements were performed at a chord Reynolds number of 5.3×10^5, corresponding to a freestream velocity of about 40 m/s. For comparison, measurements performed by Devenport et al.[15] in the undisturbed vortex wake of the generator blade at 5-deg angle of attack have been included in some of the figures.

Overall Form of the Interaction

To document the evolution of the turbulent flowfield surrounding the vortex, mean velocity and turbulence measurements were made from $0.16c$ to $15c$ downstream of the interaction blade trailing edge at $x/c = 15.16$, 15.95, 17.5, 20, 22.5, 25, and 30. At all seven locations, cross-sectional measurements were made in the y–z plane. Contours of turbulence kinetic energy and mean axial vorticity are shown in Figs. 2 and 3. The initial effect of the blade on the vortex is to cut it in two. At $x/c = 15.16$, the turbulence contours (Fig. 2) clearly show how the blade wake bisects the spiral arm of the vortex. Note that there is some dislocation of the spiral across the blade wake caused by differing spanwise velocities above the suction and below the pressure side surfaces of the blade. This $\partial V/\partial z$ contributes significantly to the streamwise vorticity ($\Omega_x = \partial W/\partial y - \partial V/\partial z$) resulting in the region of negative vorticity centered at approximately $z/c = -0.25$, seen in Fig. 3. The blade sheds negative vorticity in response to local angle-of-attack variations produced by the vortex. In the immediate vicinity of the core, $\partial\alpha/\partial y$ is negative and, thus, negative vorticity is shed. Initially, at $x/c = 15.16$, the region of negative vorticity spans over one chord.

Progressing downstream, the vortex and blade wake begin to interact. Most noticeable is the tongue of turbulent fluid that forms in the region of strongest negative vorticity between $x/c = 15.95$ and 17.5 (near $y/c = 0.55$, $z/c = -0.05$). Turbulence kinetic energy levels in the center of this region at $x/c = 17.5$ are 2.5 times as large as those in the undistorted sections of blade wake far from the vortex core. Another feature of the flow noticeable at the locations $x/c = 15.16$, 15.95, and 17.5 is the thicker, more turbulent blade wake outboard of the vortex center (more negative y) than inboard. This is consistent with the expected flow over the blade, where outboard of the vortex there is an increase in the local angle of attack, thereby increasing the thickness of the suction side boundary layer and the resulting wake, possibly to the extent that local separation occurs. Lifting of fluid away from the blade surface by the rotational motion of the vortex may also increase the wake thickness inboard of the vortex center, but this effect is clearly smaller here.

Farther downstream, the region of negative vorticity continues to distort with the blade wake. The vorticity levels decrease rapidly presumably because of turbulent mixing and cancellation with the positive vorticity distributed throughout the rest of the vortex flow. This region ultimately disappears between $x/c = 25$ and 30. However, the region of intense new turbulence continues to grow, engulfing the core and producing a large turbulent region surrounding it. Confirming that this is new turbulence, rather than a simple roll-up of the blade wake, are contours of turbulence kinetic energy production, which are shown for $x/c = 17.5$ in Fig. 4. Turbulence production in the region of strongest negative vorticity is an order of magnitude larger than in the undisturbed portion of the blade wake. Peak turbulence levels in the parts of the blade wake farthest from

Table 2 Uncertainty in velocity measurements calculated for 20:1 odds at typical locations

Quantity	Uncertainty	
	Wake	Core
U/U_∞	0.015	0.015
V/U_∞	0.015	0.015
W/U_∞	0.015	0.015
$\overline{u^2}/U_\infty^2$	3.1×10^{-6}	1.4×10^{-5}
$\overline{v^2}/U_\infty^2$	9.5×10^{-6}	1.5×10^{-5}
$\overline{w^2}/U_\infty^2$	9.9×10^{-6}	2.0×10^{-5}
$\overline{uv}/U_\infty^2$	4.3×10^{-6}	1.4×10^{-5}
$\overline{vw}/U_\infty^2$	4.5×10^{-6}	2.3×10^{-5}
$\overline{uw}/U_\infty^2$	2.9×10^{-6}	8.5×10^{-6}

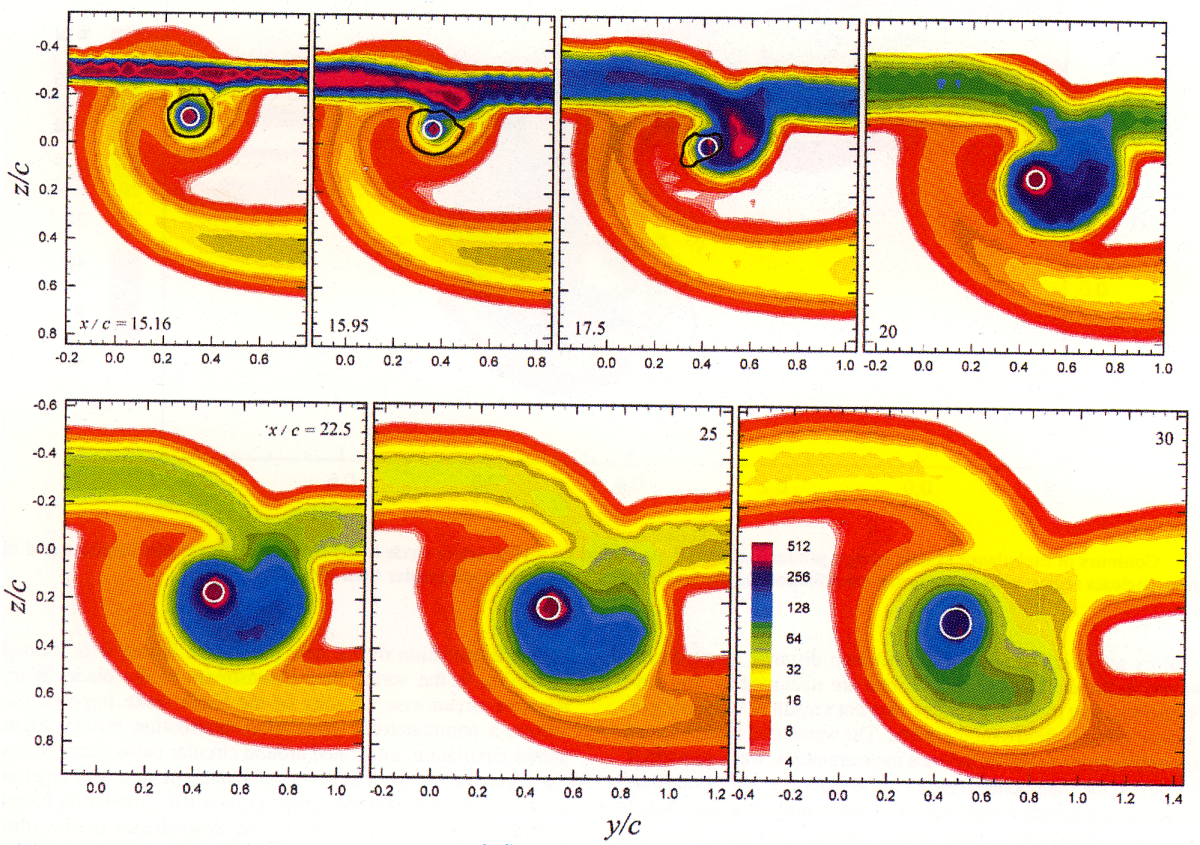

Fig. 2 Contours of turbulence kinetic energy ($k/U_\infty^2 \times 10^5$): white circles indicate core diameter, and location and black contours enclose regions where wandering contributions are greater than 30%. (No such regions exist for $x/c > 17.5$.)

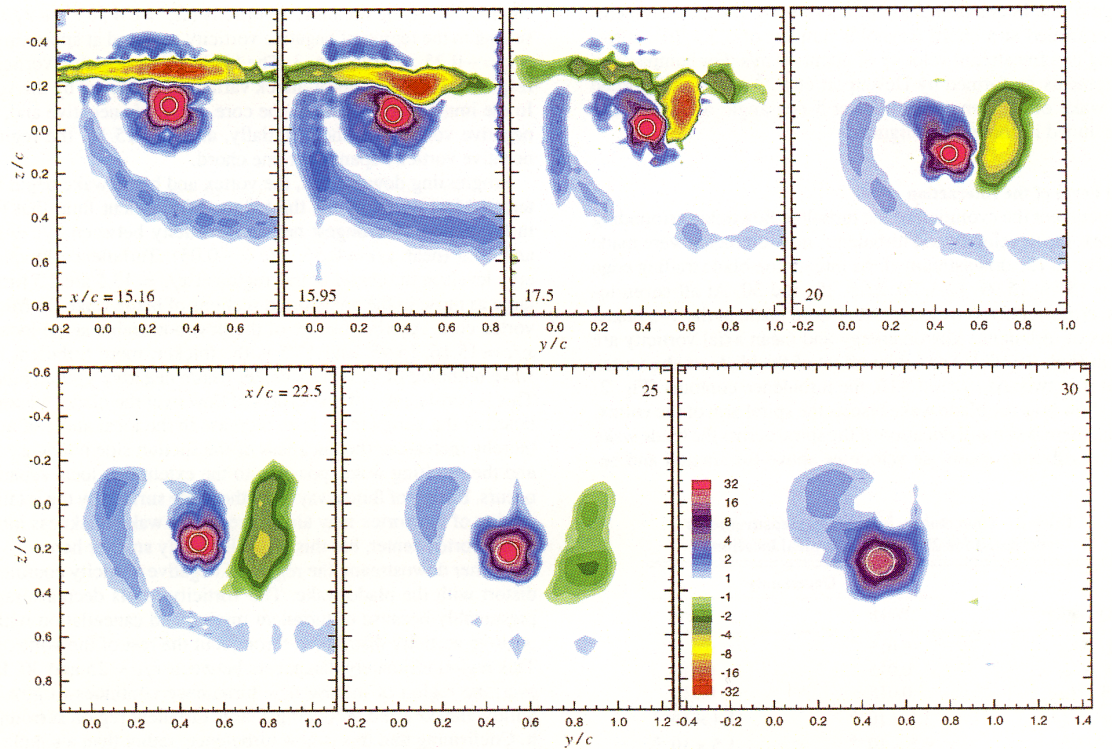

Fig. 3 Contours of mean axial vorticity ($\Omega_x c/U_\infty \times 10$): white circles indicate core diameter and location.

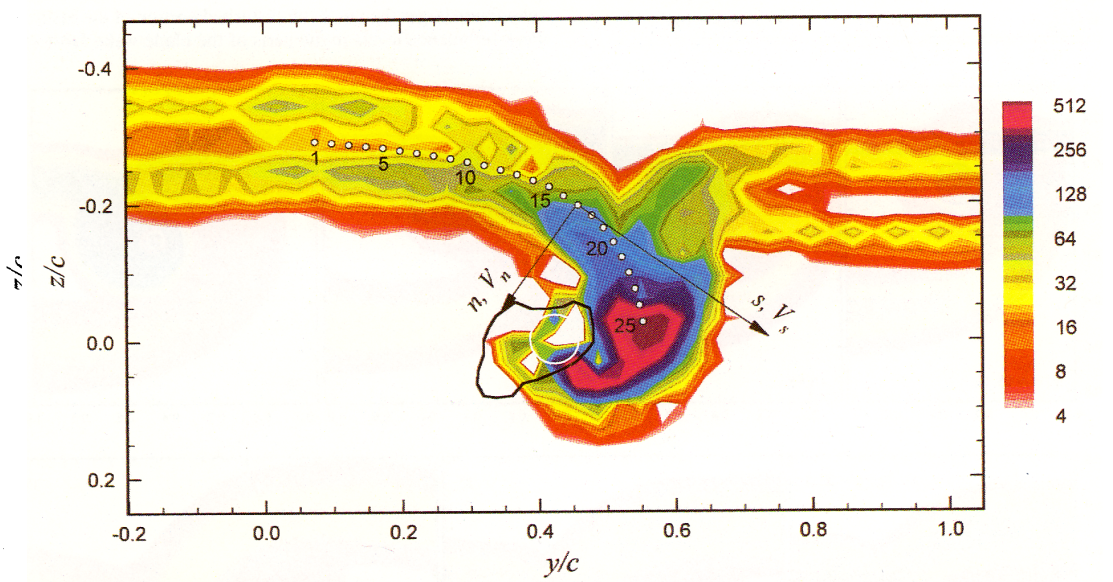

Fig. 4 Contours of turbulence kinetic energy production ($Pc/U_\infty^3 \times 10^5$) at $x/c > 17.5$: white circle indicates core diameter and location, and black contour encloses region where wandering contributions to the turbulence kinetic energy are greater than 30%.

the vortex are decreasing with downstream distance as expected; however, in the distorted portion, levels are sustained by this production. Note that these observations are not a result of wandering of the vortex velocity field over the probe. The wandering motions, and their contributions to the turbulence measurements, were quantified according to the method and results of Devenport et al.[15] Contributions to the turbulence kinetic energy were found to be significant only in the immediate vicinity of the core at $x/c = 15.16$, 15.95, and 17.5 (see Figs. 2 and 4).

One explanation of the new turbulence is that it is formed by instability in the vortex flow downstream of the blade. With the negative streamwise vorticity of the blade wake imposed on the vortex, a nonmonotonic circulation distribution results. Figure 5 shows circulation, integrated around circular paths concentric with the vortex center from the y–z plane data, plotted as a function of radius. In the undisturbed vortex ($x/c = 10$), circulation increases continuously with radius. However, downstream of the interaction ($x/c \geq 15.16$), the negative streamwise vorticity shed by the

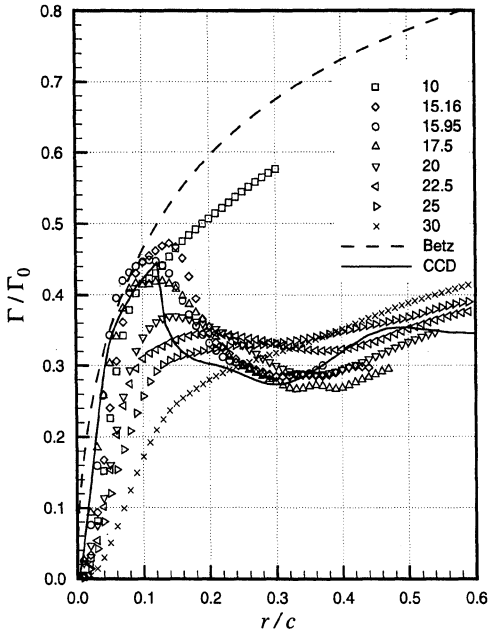

Fig. 5 Circulation distributions estimated from *y*–*z* plane data. Numbers in legend are *x/c* locations; lines are for Betz's theory and the predicted combined circulation distribution (CCD) calculated with $\Delta C_{L_{max}} = 0.2$.

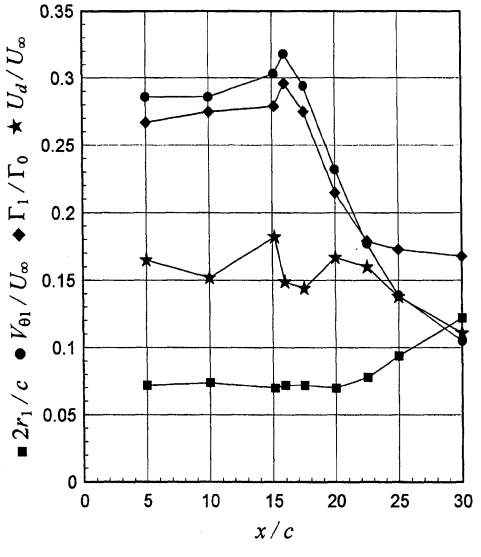

Fig. 6 Vortex core parameters as a function of downstream distance.

interaction blade greatly reduces circulation for $r/c > 0.15$, producing a strongly nonmonotonic variation. Nonmonotonic circulation distributions are unstable according to Rayleigh's criterion and, thus, are expected to produce turbulence and rapidly to diffuse. Indeed, downstream of $x/c = 17.5$, the peak in the circulation distribution begins to diffuse, and by $x/c = 25$, the distribution has regained a monotonic form. The intense production seen at $x/c = 17.5$ and other locations[10] may, therefore, be associated with this instability.

An alternative explanation (proposed by one of the reviewers of this paper) is that the new turbulence may be generated by the interaction between the vortex and small-scale turbulence in the blade wake. Specifically, vortex cores have been observed to organize small-scale turbulence into ringlike organized structures.[16] Such structures may cause intermittent busts of vorticity to be ejected from the core,[17,18] increasing its rate of diffusion.

The development of the vortex core parameters (radius, peak tangential velocity, circulation, and centerline axial velocity deficit), shown in Fig. 6, were obtained from the detailed *z*-wise profiles through the core center shown in Fig. 7. Coherent wandering motions of the vortex had a small effect on the measured values of

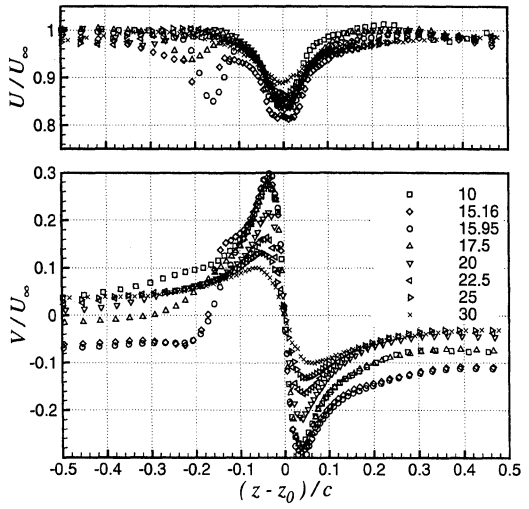

Fig. 7 Mean axial and tangential velocity profiles as a function of downstrean distance; numbers in legend are *x/c* values.

the core parameters, which was corrected for using the method of Devenport et al.[15] Corrections were typically about −5% on r_1 and 6% on V_{θ_1}, but were negligible on U_d. Immediately downstream of the blade, little change is seen in the core parameters even though the blade–vortex separation was only 3.7 core radii. The core radius remains fairly uniform until $x/c = 20$, with a small increase seen at $x/c = 22.5$, and then increases roughly linearly to a size about 67% larger than the undisturbed value. The effects of the interaction on the tangential velocity field of the vortex core are felt significantly farther upstream: There is a slight increase in peak tangential velocity immediately after the interaction, but it decreases steadily after $x/c = 15.95$ to 37% of the undisturbed value at $x/c = 30$. These changes result in the core circulation falling quickly between $x/c = 17.5$ and 22.5 likely due to the incorporation of the nearby negative vorticity into the core. A similar delay between the fall in the peak tangential velocity and the growth of core radius is also seen in the temporal variation of a Taylor vortex (which also has a region of negative vorticity surrounding its core) as calculated by Sreedhar and Ragab.[19]

Interestingly, the recovery to a monotonic circulation distribution does not appear to be accompanied by a return to vortex stability. The rapid decay of the core triggered by the nonmonotonic circulation distribution causes the peak tangential velocity to fall slightly below the centerline axial velocity deficit at $x/c = 30$. According to the stability computations of Mayer and Powell[20] and direct numerical simulations by Ragab and Sreedhar,[21] such a vortex is marginally unstable.

Circulation Predictions

Possibly the most interesting feature of the flow is the negative vorticity, which is shed by the interaction blade as a result of the angle-of-attack variation induced by the passing vortex (see Fig. 3). This may be predicted to a degree using an adaptation to Prandtl's lifting line theory following the work of Hancock,[22] who derived the loading produced by a free line vortex passing above a two-dimensional wing.

Consider a vortex of arbitrary circulation distribution passing perpendicular to a geometrically untwisted blade constrained at each end by infinite flat plates, as shown in Fig. 8. The effects of the nonuniform inflow produced by the vortex are assumed to be the same as those of a twist on the blade with the twist angle distribution being equal to the flow angle distribution $\alpha_v(y)$ produced by the vortex. Using the coordinates shown in Fig. 8 we write

$$\alpha_v(y) = \arctan\left(\frac{-W}{U_\infty}\right) \approx \frac{\Gamma_i(r)(y_v - y)}{2\pi r^2 U_\infty} \tag{1}$$

where $r = \sqrt{[\Delta^2 + (y_v - y)^2]}$. The complete angle-of-attack distribution for the blade is $\alpha(y) = \alpha_b + \alpha_v(y)$.

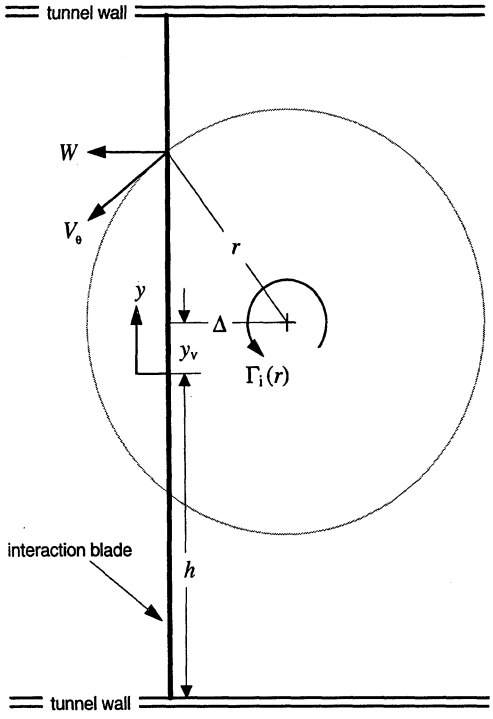

Fig. 8 Geometry and coordinates used in derivation of theoretical shed vorticity distribution.

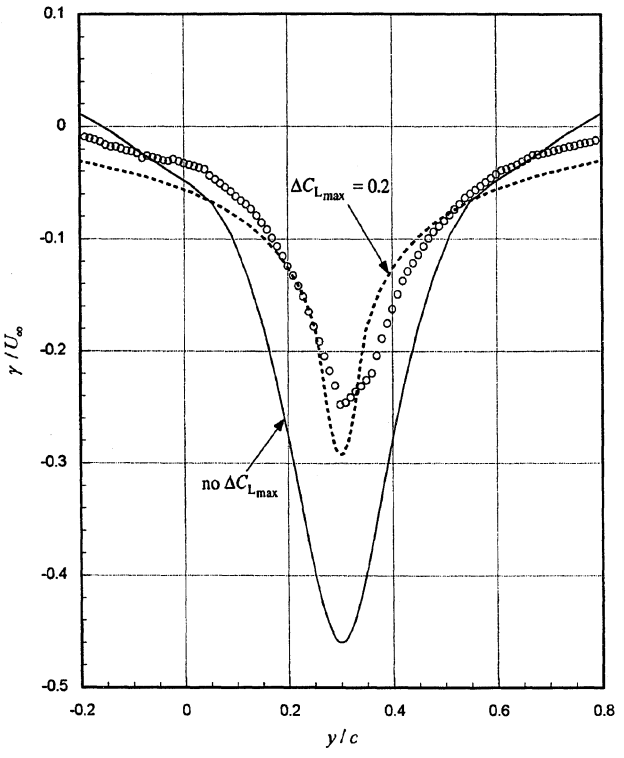

Fig. 9 Comparison between theoretical and measured shed vortex sheet strengths; experimental data (symbols) from y–z plane measurements at $x/c = 15.16$.

The lifting line theory equations used to compute the shed vortex sheet strength distribution from $\alpha(y)$ depend on the configuration. In the present situation of a blade that completely spans the wind-tunnel walls, the relationship between $\alpha(y)$ and the blade circulation distribution $\Gamma_b(y)$ is

$$\alpha(y) = \frac{\Gamma_b(y)}{\pi c U_\infty} + \frac{1}{4\pi U_\infty}\int_{-\infty}^{\infty} \frac{1}{y - y'}\frac{d\Gamma_b}{dy'}\,dy' \tag{2}$$

The reflections provided by the wind-tunnel walls will result in the $\Gamma_b(y)$ being periodic over twice the distance between the walls. Under these conditions, the solution to this equation is the series

$$\Gamma_b(y) = bU_\infty\left\{\alpha_b\frac{\pi c}{b} + \sum_{n=1,\ldots,\infty} A_n\left(\frac{b}{\pi c} + \frac{n\pi}{4}\right)^{-1} \times \cos\left[\frac{n\pi}{b}(y+h)\right]\right\} \tag{3}$$

where b and h are defined in Fig. 8 and the A_n are coefficients in the Fourier cosine series for $\alpha(y)$, i.e.,

$$\alpha(y) = \alpha_b + \sum_{n=1,\ldots,\infty} A_n \cos\left[\frac{n\pi}{b}(y+h)\right] \tag{4}$$

This solution is quite different than the solution for a blade with a finite span in external flow. Now the strength of the vortex sheet shed from the blade can be calculated as

$$\gamma_b(y) = -\frac{d\Gamma_b}{dy} = \pi U_\infty \sum_{n=1,\ldots,\infty} nA_n\left(\frac{b}{\pi c} + \frac{n\pi}{4}\right)^{-1} \times \sin\left[\frac{n\pi}{b}(y+h)\right] \tag{5}$$

The predicted shed vorticity distribution is, therefore, independent of α_b, which, given the limitations of this analysis, implies that the consequences of its downstream interaction with the vortex should be independent of the blade angle of attack.

Two calculations of the vortex sheet strength are shown in Fig. 9 for a blade–vortex separation of $|\Delta/c| = 0.125$. The first is a direct evaluation of Eqs. (4) and (5) using the measured undisturbed generator vortex circulation distribution at $x/c = 10$ (see Fig. 5).

Another calculation was done with a limit of 0.2 imposed on the change in lift coefficient that can be experienced by the blade. The idea of imposing a limit is based on the research of Ham,[23] which suggests that the spanwise pressure gradient supplied by the vortex limits, through flow separation, the amount of loading that can be induced on the blade. For typical helicopter rotor BVIs, Ham states that this limits the maximum incremental lift coefficient to the order of 0.2–0.3. To estimate the shed vorticity distribution from the experimental data, the y–z plane measurements made at $x/c = 15.16$ were used. The vortex sheet strength is simply the difference in the V component of velocity on either side of the sheet. Because the sheet actually has a finite thickness, its strength is dependent on the choice of its edges. We have chosen the lines $z/c = -0.2$ and -0.35, which appear to bound the blade wake fluid (see Figs. 2 and 3). Figure 9 shows that the theoretical distribution without any limit on $\Delta C_{L_{max}}$ significantly overpredicts the strength of the shed vorticity; however, with $\Delta C_{L_{max}} = 0.2$, the theoretical distribution matches the shape and levels of the measured distribution surprisingly well. Obviously, additional experimental sheet strength data for different blade–vortex separations, vortex strengths, and interaction blade angles of attack are needed to completely validate the usefulness of this model. It is likely that the $\Delta C_{L_{max}}$ parameter will be dependent on the blade angle of attack and the blade–vortex separation (which changes the extent of the spanwise flow on the blade).

The experimental data show that the shed vorticity has a profound effect on the circulation distribution of the vortex. By the use of a method similar to Betz's[24] theory, the circulation distribution of the vortex downstream of the interaction can be predicted. It is assumed that the vorticity contained by an incremental portion of the vortex sheet lying at a distance r from the vortex center remains at this distance, but becomes distributed into an annulus. The final circulation distribution of the vortex, is therefore, $\Gamma_f(r) = \Gamma_i(r) + \delta\Gamma(r)$, where $\delta\Gamma(r)$ is the additional circulation provided by the vortex sheet at $r > \Delta$, which can be calculated as

$$\delta\Gamma(r) = \int_{\sqrt{r^2-\Delta^2}}^{-\sqrt{r^2-\Delta^2}} \frac{d\Gamma_b}{dy}\,dy = 2\Gamma_b(\sqrt{r^2-\Delta^2}) \tag{6}$$

Figure 5 shows a comparison between predicted circulation distributions and the distributions calculated from the y–z plane measurements. The predicted distribution with $\Delta C_{L_{max}} = 0.2$

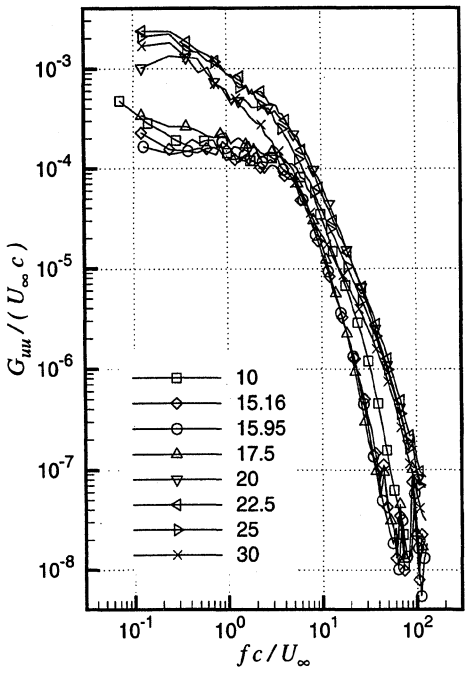

Fig. 10 Axial velocity component autospectra at the core center normalized on freestream velocity and chordlength as a function of downstream distance (*x/c* values listed in legend).

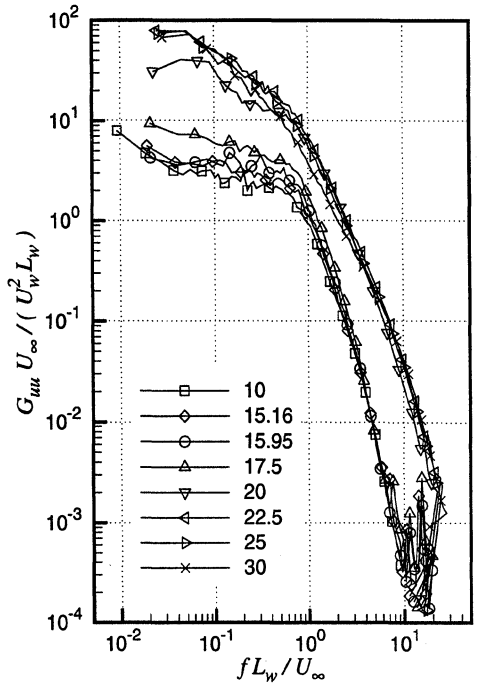

Fig. 11 Axial velocity component autospectra at the core center normalized on vortex generator wake scales at various locations downstream (*x/c* values in legend).

matches the measured distributions for $x/c < 20$ well. These measured distributions do not change significantly even though the vorticity field (see Fig. 3) is being distorted. This supports the assumption that the vorticity contained in the interaction blade wake remains at a constant distance from the vortex center even though the fluid associated with this vorticity is highly turbulent. It is not until the vortex core becomes turbulent at $x/c = 20$ that a marked change in the circulation distribution is seen.

Spectral Decomposition

Velocity autospectra were measured in the vortex core center at each location downstream of the interaction. Axial component autospectra normalized on freestream velocity and chord length as a function of downstream distance are shown in Fig. 10. For a while following the interaction ($x/c = 15.16$, 15.95, and 17.5), the rolloff of the autospectra at high frequencies ($fc/U_\infty > 6$) is similar to the undisturbed vortex suggesting that the structure of the core is unchanged. Devenport et al.[14] provide detailed evidence that the undisturbed vortex core is laminar. In particular, the rotational motion of the core would tend to supress high-frequency velocity fluctuations, and the stress field of the core is well predicted by coherent wandering of the mean velocity field.

Farther downstream ($x/c \geq 20$), autospectra appear to indicate that a significant change in the spectral signature of vortex core has occurred. Levels at all frequencies jump up at least one-half a decade, and a short inertial subrange ($-\frac{5}{3}$ slope) develops. These changes may signal that the core has become turbulent. Spectral levels at frequencies above $fc/U_\infty = 20$ are at least an order of magnitude greater than those seen upstream at $x/c = 15.16$–17.5. This change in signature corresponds directly to the growth of the core radius, which is seen to occur shortly after $x/c = 20$.

The jump in spectral levels and the change in spectral shape seen between $x/c = 17.5$ and 30 persists regardless of the manner in which the spectra are normalized. However, different normalizations do provide a measure of collapse of the spectra for $x/c \leq 17.5$ and for $x/c \geq 20$ implying some scaling of the velocity fluctuations. (See Ref. 10 for several normalizations.) The normalizations presume that the convective velocity of any disturbances should be close to U_∞.

The best normalization for locations $x/c \leq 17.5$ was obtained using the velocity and length scales of the generator wake (Fig. 11) that were obtained from the isolated vortex study by Devenport et al.[15] Their data indicated that the evolution of the axial velocity and turbulence profiles in the flat portion of the wake far from the core was well described by only one length and one velocity scale (L_w and U_w), which grow and decay, respectively, approximately as the square root of the streamwise distance. Using this normalization, the autospectra collapse onto two distinct bands. For frequencies $fL_w/U_\infty > 2$, the spectra for $x/c = 10$, 15.16, 15.95, and 17.5 collapse onto nearly the same curve. The collapse of the curves farther downstream ($x/c \geq 20$) is not easily explained and is most likely coincidence. Devenport et al.[15] conclude that this scaling works in the case of the undisturbed vortex because the velocity fluctuations in the laminar flow core are the result of inactive motions produced as it is buffeted by the surrounding wake turbulence. The length and velocity scales of the highly turbulent blade wake might, therefore, be more appropriate scales for $x/c \geq 20$. Alternatively, if the velocity fluctuations in the disturbed core are a consequence of turbulence generated by its rotational motion, V_{θ_1} and r_1 would seem to be appropriate scales. However, neither of these scalings produces significant collapse of the spectra. Only scales based on the axial velocity deficit profile of the vortex core produce much collapse of the spectra for $x/c \geq 20$ (Ref. 10), the collapse being best in the midfrequency inertial subrange.

Turbulence Kinetic Energy Production

The interaction between the positive vorticity of the vortex and the negative vorticity of the blade wake has been identified as a likely cause of the turbulence kinetic energy production. A close look at the contours of turbulence kinetic energy production is shown in Fig. 4. A series of points evenly spaced by $0.025c$ has been identified on the contours, which starts in the center of the nearly two-dimensional portion of the interaction blade wake and follows the ridge of maximum axial normal stress levels (indicative of the wake centerline) toward the peak at (0.55, −0.03). Obviously, without the effects of the interaction there would be no changes along this path. At each point, an aligned coordinate system is defined such that the s direction is tangent to the curve that passes through the points and the n direction points toward the center of curvature. (Mean velocities in the s and n directions are denoted V_s and V_n, respectively. Fluctuating velocities in the s and n directions are denoted v_s and v_n, respectively.) The turbulence kinetic energy production in this coordinate system is

$$P = \left(\overline{v_n^2} - \overline{v_s^2}\right)\frac{\partial V_s}{\partial s} - \overline{uv_s}\frac{\partial U}{\partial s} - \overline{uv_n}\frac{\partial U}{\partial n} - \overline{v_s v_n}\left(\frac{\partial V_n}{\partial s} + \frac{\partial V_s}{\partial n}\right) \tag{7}$$

if streamwise derivatives are ignored and continuity is satisfied.

Production remains roughly uniform between locations 1 and 5, but increases rapidly between locations 5 and 22, where the wake has been significantly distorted by the vortex. The two terms $-\overline{uv_s}(\partial U/\partial s)$ and $-\overline{uv_n}(\partial U/\partial n)$ have negligible contributions along this path, which is almost entirely due to the in-plane stresses multiplying the rates of stretching $(\partial V_s/\partial s)$ and skewing $(\partial V_n/\partial s + \partial V_s/\partial n)$. [Note $-\overline{uv_n}(\partial U/\partial n)$ is certainly the main source of production in the two-dimensional wake away from its centerline.] These strain rates produced by the rotating velocity field of the vortex increase along the path to reach maxima near location 25, where the blade wake appears to form a cusp. The corresponding stress terms, $\overline{v_n^2} - \overline{v_s^2}$ and $\overline{v_s v_n}$, also become larger along the path, a symptom of the growing anisotropy of the Reynolds stress tensor as one moves from the undisturbed blade wake to the cusped region.[10] The stretching of the in-plane vorticity of large energy containing eddies is a likely cause of this anisotropy.

Conclusions

Experiments were performed to document the turbulent flowfield resulting from the interaction of a streamwise vortex with a NACA 0012 airfoil (referred to as the *blade*) at 5-deg angle of attack in incompressible flow. The configuration was arranged so that the vortex missed the blade by $0.125c$, passing to the pressure side. Detailed three-component velocity and turbulence measurements were made using a miniature four-sensor hot-wire probe to document the downstream development of the vortex.

The vortex passes the blade without immediate change in the form and structure of its core. Outside the core, the flow is modified by the blade wake, which bisects the spiral arm of the vortex. The blade wake contains a significant amount of negative streamwise vorticity produced by the angle-of-attack distribution induced by the passing vortex. This negative vorticity and the turbulent motions of the blade wake appear to trigger the rapid decay of the vortex. Specifically, a tongue of turbulent fluid formed initially in the region of peak negative vorticity grows rapidly to engulf the core stimulating an increase in it size, a reduction in its strength, and a loss of circulation as its vorticity is partially cancelled by the blade wake. The manner in which these changes occur bears at least a passing resemblance to the turbulent decay of a Taylor vortex. As the core decays, the circulating velocity field outside it winds up the remainder of the blade wake, further increasing the size of the turbulent region in which the core has become embedded.

A simple theoretical model has been developed using modified forms of Prandtl's lifting line theory and Betz's theory. The model predicts the circulation distribution on the blade in the presence of the vortex and, thus, the strength of the negative vorticity shed into the blade wake. With an empirical limit imposed on the change in local blade lift coefficient that the vortex may produce, the model quite accurately predicts the measured vortex sheet strength and circulation distribution in the vortex immediately following the interaction. The model also shows that the shed vortex sheet strength is independent of blade angle of attack. Therefore, we expect blade angle of attack to be only a weak factor in the development of a vortex downstream of a perpendicular blade vortex interaction.

Acknowledgments

The authors would like to thank NASA Langley Research Center, in particular Thomas F. Brooks and Casey L. Burley, for their work under Grant NAG-1-1539. The assistance of Gordon Follin and Mark Engel in taking many of the measurements presented here is also gratefully acknowledged.

References

[1]Widnall, S. E., and Wolf, T. L., "Effect of Tip Vortex Structure on Helicopter Noise Due to Blade–Vortex Interaction," *Journal of Aircraft*, Vol. 17, No. 10, 1980, pp. 705–711.

[2]Srinivasan, G. R., McCroskey, W. J., and Baeder, J. D., "Aerodynamics of Two-Dimensional Blade–Vortex Interaction," AIAA Paper 85-1560, July 1985.

[3]Tadghighi, H., Hassan, A. A., and Charles, B., "Prediction of Blade–Vortex Interaction Noise Using Airloads Generated by a Finite-Difference Technique," *Journal of the American Helicopter Society*, Vol. 37, No. 4, 1992, pp. 38–47.

[4]Lee, D. J., and Smith, C. A., "Distortion of Vortex Core During Blade/Vortex Interaction," AIAA Paper 87-1243, June 1987.

[5]Brooks, T. F., Marcolini, M. A., and Pope, D. S., "Main Rotor Broadband Noise Study in the DNW," *Journal of the American Helicopter Society*, Vol. 34, No. 2, 1989, pp. 3–12.

[6]Glegg, S. A. L., "The Prediction of Blade–Wake Interaction Noise Based on a Turbulent Vortex Model," *AIAA Journal*, Vol. 29, No. 10, 1991, pp. 1545–1551.

[7]Glegg, S. A. L., and Devenport, W. J., "The Application of Experimental Data to Blade Wake Interaction Noise Prediction," *Unsteady Aerodynamics, Aeroacoustics and Aeroelasticity of Turbomachines and Propellers*, edited by H. M. Atassi, Springer, New York, 1992, pp. 705–723.

[8]Wittmer, K. S., Devenport, W. J., and Rife, M. C., "Perpendicular Blade Vortex Interaction," *AIAA Journal*, Vol. 33, No. 9, 1995, pp. 1667–1674.

[9]Devenport, W. J., Glegg, S. A. L., Wittmer, K. S., and Rife, M. C., "Perpendicular Blade Vortex Interaction and Its Implications for Helicopter Noise Prediction," Dept. of Aerospace and Ocean Engineering, Virginia Polytechnic Inst. and State Univ., Rept. VPI-AOE 214, Blacksburg, VA, Aug. 1993.

[10]Wittmer, K. S., "Turbulent Flowfield Downstream of a Perpendicular Airfoil–Vortex Interaction," Ph.D. Dissertation, Dept. of Aerospace and Ocean Engineering, Virginia Polytechnic Inst. and State Univ., Blacksburg, VA, Oct. 1996.

[11]Wittmer, K. S., Devenport, W. J., and Glegg, S. A. L., "Effects of Perpendicular Blade–Vortex Interaction, Part 2: Parameter Study," *AIAA Journal*, Vol. 37, No. 7, 1999, pp. 813–817.

[12]Choi, K., and Simpson, R. L., "Some Mean-Velocity, Turbulence, and Unsteadiness Characteristics of the VPI&SU Stability Wind Tunnel," Dept. of Aerospace and Ocean Engineering, Virginia Polytechnic Inst. and State Univ., Rept. VPI-AOE-161, Blacksburg, VA, Dec. 1987.

[13]Kovasznay, L. S. G., *Physical Measurements in Gas Dynamics and Combustion*, Princeton Univ. Press, Princeton, NJ, 1954, p. 227.

[14]Wittmer, K. S., Devenport, W. J., and Zsoldos, J. S., "A Four-Sensor Hot-Wire System for Three-Component Velocity Measurement," *Experiments in Fluids*, Vol. 24, No. 5/6, 1998, pp. 416–423.

[15]Devenport, W. J., Rife, M. C., Liapis, S. I., and Follin, G. J., "The Structure and Development of a Wing-Tip Vortex," *Journal of Fluid Mechanics*, Vol. 312, Jan. 1996, pp. 67–106.

[16]Melander, M. V., and Hussain, F., "Coupling Between a Coherent Structure and Fine Scale Turbulence," *Physical Review E*, Vol. 48, No. 4, 1993, pp. 2669–2689.

[17]Bandyopadhyay, P. R., Stead, D. J., and Ash, R. L., "Organized Nature of a Turbulent Trailing Vortex," *AIAA Journal*, Vol. 29, No. 10, 1991, pp. 1627–1633.

[18]Sarpkaya, T., "Three-Dimensional Interactions of Vorticies with a Free Surface," AIAA Paper 92-0059, Jan. 1992.

[19]Sreedhar, M. K., and Ragab, S. A., "Large Eddy Simulation of a Longitudinal Vortex," AIAA Paper 94-0529, Jan. 1994.

[20]Mayer, E. W., and Powell, K. G., "Similarity Solutions for Viscous Vortex Cores," *Journal of Fluid Mechanics*, Vol. 238, 1992, pp. 487–507.

[21]Ragab, S. A., and Sreedhar, M. K., "Numerical Simulation of Vortex with Axial Velocity Deficits," *Physics of Fluids*, Vol. 7, No. 3, 1995, pp. 549–558.

[22]Hancock, G. J., "Aerodynamic Loading Induced on a Two-Dimensional Wing by a Free Vortex in Incompressible Flow," *Aeronautical Journal of the Royal Aeronautical Society*, Vol. 75, June 1971, pp. 413–416.

[23]Ham, N. D., "Some Conclusions from an Inverstigation of Blade–Vortex Interaction," *Journal of the American Helicopter Society*, Vol. 20, No. 4, 1975, pp. 26–31.

[24]Betz, A., "Behavior of Vortex Systems," NACA TM-713, June 1933.

P. R. Bandyopadhyay
Associate Editor